PNAS RESEARCH ARTICLE | BIOCHEMISTRY

A specialized integrin-binding motif enables proTGF-β2 activation by integrin αVβ6 but not αVβ8

Viet Q. Le[a,b,1], Bo Zhao[a,b,1,2], Siddanth Ramesh[a], Cameron Toohey[a], Adam DeCosta[a], Julian Mintseris[c], Xinyue Liu[c], Steven Gygi[c], and Timothy A. Springer[a,b,3]

Edited by William DeGrado, University of California San Francisco, San Francisco, CA; received March 27, 2023; accepted April 28, 2023

Activation of latent transforming growth factor (TGF)-β2 is incompletely understood. Unlike TGF-β1 and β3, the TGF-β2 prodomain lacks a seven-residue RGDLXX (L/I) integrin-recognition motif and is thought not to be activated by integrins. Here, we report the surprising finding that TGF-β2 contains a related but divergent 13-residue integrin-recognition motif (YTSGDQKTIKSTR) that specializes it for activation by integrin αVβ6 but not αVβ8. Both classes of motifs compete for the same binding site in αVβ6. Multiple changes in the longer motif underlie its specificity. ProTGF-β2 structures define interesting differences from proTGF-β1 and the structural context for activation by αVβ6. Some integrin-independent activation is also seen for proTGF-β2 and even more so for proTGF-β3. Our findings have important implications for therapeutics to αVβ6 in clinical trials for fibrosis, in which inhibition of TGF-β2 activation has not been anticipated.

transforming growth factor beta | integrins | X-ray crystallography

Transforming growth factor-βs (TGF-β) regulate development, homeostasis, and disease processes including fibrosis (1–4). TGF-βs are synthesized as latent prodomain–growth factor complexes (e.g., proTGF-βs) in association with a milieu anchor protein (5). After deposition on cell surfaces or in the extracellular matrix, release of the growth factor from the prodomain is required for signaling. TGF-β1 and β3 are activated by integrins αVβ6 and αVβ8, which bind to an RGDLXX (L/I) motif in their prodomains (6–8). In contrast, TGF-β2 lacks such a motif and has been widely assumed to be resistant to integrin-mediated activation.

Results

Integrin αVβ6 Robustly Activates Latent TGF-β2. We screened multiple integrins for their ability to activate TGF-β2. Activation was measured using an assay in which HEK293 cells stably transfected with the CAGA-luciferase reporter (9) were cocultured with i) Expi293 cells transfected with various integrins and ii) Expi293 cells cotransfected with TGF-β2 and one of the following milieu anchors: glycoprotein A repetitions predominant (GARP), latent TGF-β binding protein 1 (LTBP1), or LTBP3. Complexes of GARP with TGF-β1, β2, and β3 localize to the cell surface (10), whereas complexes of LTBP1 and LTBP3 with TGF-β1, β2, and β3 are stored in the extracellular matrix (11). Cell surface expression of GARP/TGF-β2 complexes and each integrin was confirmed by flow cytometry (Fig. 1*A* and *SI Appendix*, Fig. S1). Integrin-independent activation of TGF-β2 was seen when GARP/TGF-β2 transfectants were cocultured with mock-transfected cells; however, coculture with αVβ6-transfectants strongly increased activation (Fig. 1*A*). In contrast, cells expressing αVβ8, the other six RGD-recognizing integrins (12), or integrin α4β1 did not activate TGF-β2. Similarly, activation of TGF-β2 coexpressed with LTBP1 or LTBP3 was mediated by αVβ6 but not αVβ8 or other integrins (Fig. 1*B*).

TGF-β1, β2, and β3 varied in their requirements for cotransfection with a milieu anchor for integrin-dependent and independent activation (Fig. 1*C*). TGF-β prodomains contain a Cys near their N termini that becomes disulfide-linked to milieu anchors in the endoplasmic reticulum, and the absence of milieu anchor cotransfection can cause poor expression, aberrant secretion (13), or association with chaperonins (14). Many previous studies of activation of TGF-β1 omitted cotransfection of a milieu anchor with TGF-β1; it has been generally assumed that transfected cells expressed a milieu anchor which enabled activation by αVβ6 and αVβ8, but the identity of this anchor has not been determined. One such study reported that αVβ6 activated TGF-β1 but not TGF-β2 (7). In agreement, we found αVβ6-dependent activation of TGF-β1 but little activation of TGF-β2 in the absence of milieu anchor cotransfection (Fig. 1*C*). Similarly to GARP, LTBP-1 and LTBP-3 supported activation of TGF-β1 by both αVβ6 and αVβ8 and activation of TGF-β2 only by αVβ6. TGF-β3 was distinctive in its high level of integrin-independent activation.

Significance

Transforming growth factor (TGF)-β regulates immune function, development, and tissue repair. The three TGF-βs are produced in an inactive, latent form that must be activated to initiate TGF-β signaling. We have found that TGF-β2 can be activated by integrin αVβ6. Unlike TGF-β1 and β3, TGF-β2 is specifically activated by integrin αVβ6 and not αVβ8. The unappreciated role of integrin αVβ6 in TGF-β2 activation fills a large gap in our understanding of TGF-β biology and has important implications for the development of safe and efficacious integrin αVβ6 therapeutics for fibrosis in which inhibition of TGF-β2 activation had not previously been considered.

Author contributions: V.Q.L., B.Z., and T.A.S. designed research; V.Q.L., B.Z., S.R., C.T., A.D., J.M., and X.L. performed research; V.Q.L., B.Z., S.R., J.M., S.G., and T.A.S. analyzed data; and V.Q.L. and T.A.S. wrote the paper.

Competing interest statement: T.A.S. is a stockholder of Morphic Therapeutic and is a founder and board member of Morphic Therapeutic.

This article is a PNAS Direct Submission.

[1]V.Q.L. and B.Z. contributed equally to this work.

[2]Present address: Molecular Cancer Research Center, School of Medicine, Shenzhen Campus of Sun Yat-sen University, Shenzhen, Guangdong, China.

[3]To whom correspondence may be addressed. Email: springer@crystal.harvard.edu.

This article contains supporting information online at https://www.pnas.org/lookup/suppl/doi:10.1073/pnas.2304874120/-/DCSupplemental.

Published June 6, 2023.

The function-blocking αVβ6-specific antibody 7.1g10 (15) inhibited activation by αVβ6 of TGF-β2 and TGF-β1 GARP complexes, thereby demonstrating the high specificity of integrin activation (Fig. 1*D*). Fitting the dose–response curve showed incomplete inhibition by 7.1g10, particularly of TGF-β2 activation, consistent with the integrin-independent component seen with mock transfectants (Fig. 1*A*).

Mutating the Asp of the RGDLXX (L/I) motif to Glu in TGF-β1 abolishes αVβ6-dependent activation (16–18). Although TGF-β2 lacks this motif, it contains an SGDQKTI motif in a similar position (Fig. 2*A*). Mutation of the Asp in this motif to Glu abolished αVβ6-dependent activation (Fig. 1*E*). Mutating the SGD motif to RGD or replacing the entire SGDQKTI sequence of TGF-β2 with RGDLATI from TGF-β1 decreased αVβ6-dependent activation by two-fold (Fig. 1*E*). In contrast, replacement with RGDLATI sensitized TGF-β2 to αVβ8-mediated activation. Thus, although TGF-β2 lacks the motif found in TGF-β1 and β3, it contains a distinct motif that enables activation

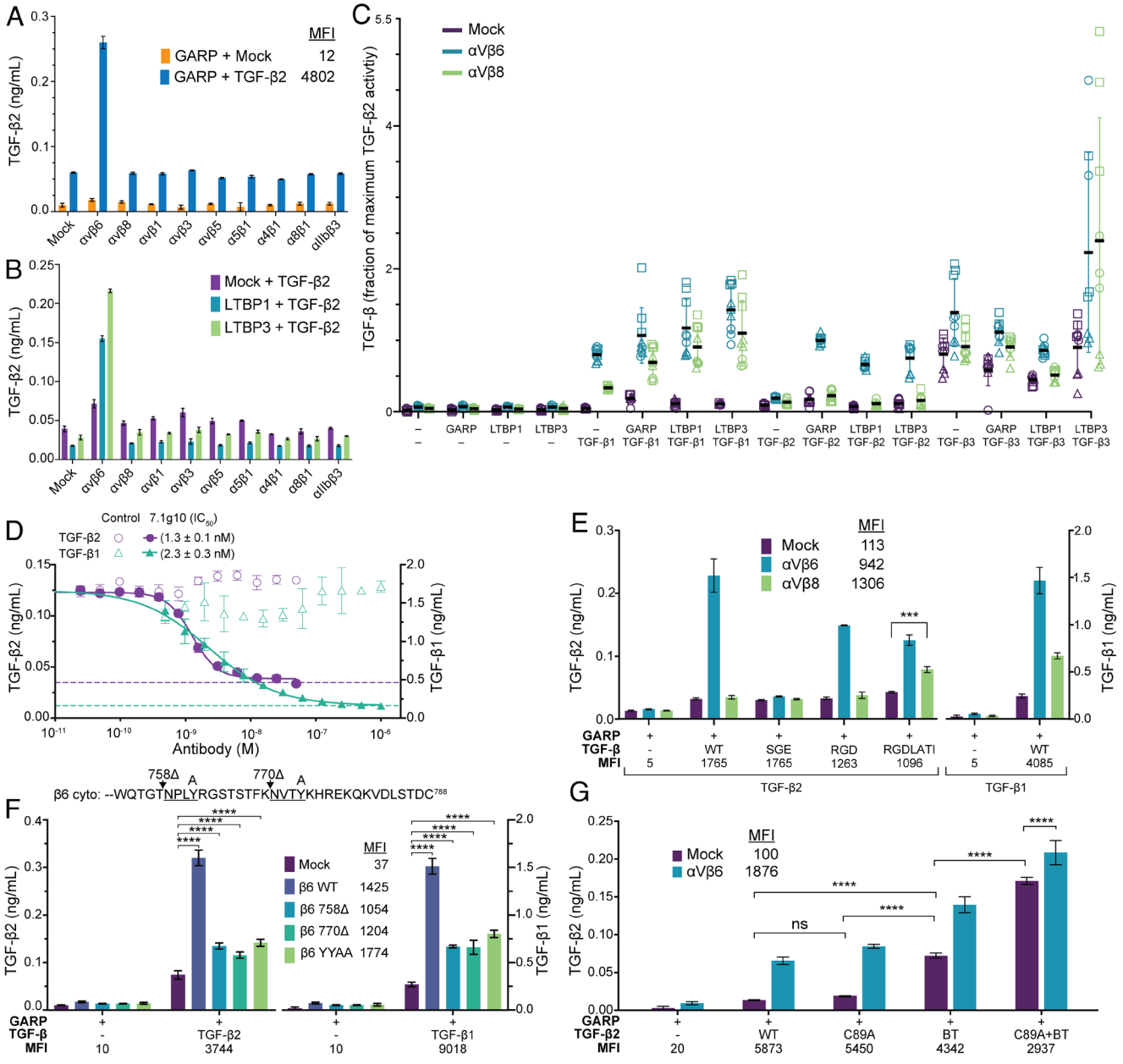

Fig. 1. Integrin αVβ6–mediated activation of TGF-β2. (*A*–*G*) CAGA luciferase reporter coculture assays characterizing integrin-mediated activation of TGF-β standardized with purified TGF-β growth factor. Median fluorescence intensities (MFI) for cell surface integrins or FLAG-tagged TGF-βs measured by FACS are reported in keys or below graphs in panels (*A* and *E*–*G*). (*A* and *B*) Integrin dependence of activation of TGF-β2 coexpressed with GARP (*A*) or alone or with LTBP1 or LTBP3 (*B*). (*C*) Effect of milieu anchor co-expression on αVβ6 and αVβ8-mediated activation of TGF-β1, TGF-β2 and TGF-β3. TGF-β activation over three independent experiments is shown as the fraction of the amount of TGF-β2 released by αVβ6 transfectants from GARP/TGF-β2 transfectants in each experiment. (*D*) Inhibition of αVβ6-mediated activation of TGF-β2 and TGF-β1 by the αVβ6 function-blocking antibody 7.1g10 or mouse IgG X63 as isotype control. IC_{50} values are from fits to a four parameter dose response curve (solid lines). Dashed lines show the levels of αVβ6-independent activation. (*E*) Effect of replacements in the SGDQKTI sequence in TGF-β2 on αVβ6-mediated activation. (*F*) Effect of truncations and mutations that eliminate talin or kindlin binding sites in the integrin β6 cytoplasmic domain on TGF-β2 activation. A segment of the integrin β6 cytoplasmic domain sequence is shown with the talin and kindlin binding sites underlined. The positions of Tyr-to-Ala mutations (A) and truncations (Δ) are indicated above the sequence. (*G*) Effect of Cys-to-Ala mutations in TGF-β2 inter-prodomain disulfides on activation. BT, bowtie triple Cys to Ala mutation. Data show mean ± SD of three biological replicates from representative experiments. Overall results from three such independent experiments are shown in *SI Appendix*, Fig. S2. *P*-values were determined using the Tukey multiple comparisons test following a two-way ANOVA (ns: $P > 0.05$, *$P < 0.05$, **$P < 0.01$, ***$P < 0.001$, ****$P < 0.0001$).

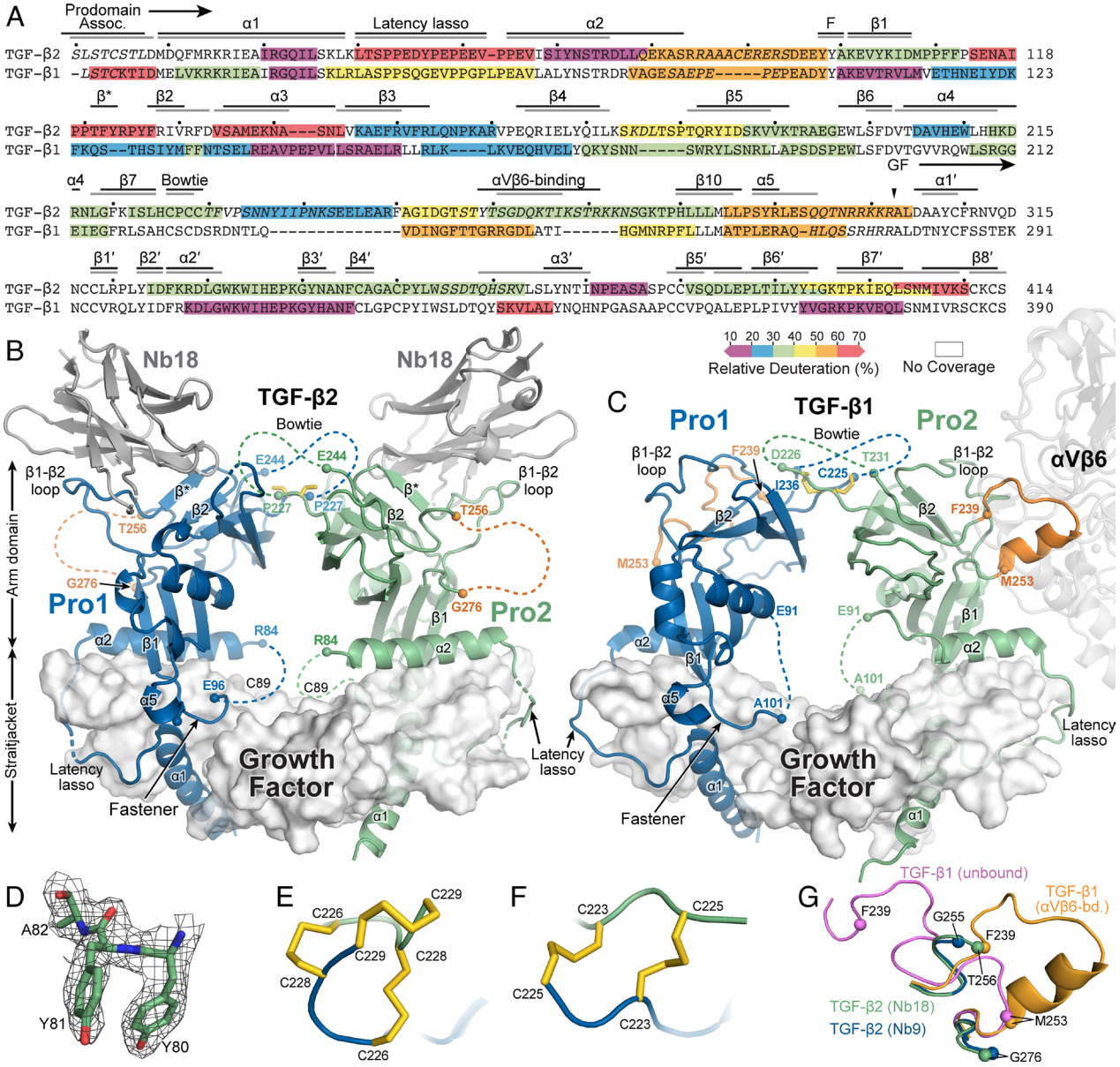

Fig. 2. ProTGF-β2 structure. (*A*) Sequence alignment of TGF-β2 and β1 with deuterium uptake after 60 s keyed to the color scale (19). Sequences of disordered regions are italicized. Numbering is based on the immature protein, and dots represent decadal positions in TGF-β2. Structural elements are labeled and shown as lines for TGF-β2 (*Upper*) and TGF-β1 (*Lower*). Assoc, association region; F, fastener; BT, bowtie; arrowhead, proconvertase cleavage site. (*B* and *C*) Crystal structures of the proTGF-β2/Nb18 complex (*B*) and proTGF-β1 with one monomer complexed with αVβ6 (PDB ID:5ffo) (*C*). Nanobodies and prodomains are shown in ribbon cartoon and growth factor domains are shown as solvent-accessible surfaces. Cysteine sidechains are shown in yellow stick. Termini that flank disordered regions are shown as Cα spheres. Integrin binding loops that are disordered in TGF-β2 are shown as orange dashes and that rearrange in TGF-β1 are depicted in orange. Other disordered regions are shown as dashes in the same color as their domains. (*D*) Electron density for the fastener element of the TGF-β2 Nb18 complex shown in stick with the 2Fo–Fc map contoured at 1σ in mesh. (*E* and *F*) The three bowtie disulfides of the TGF-β2/Nb9 complex (*E*) and the two bowtie disulfides of TGF-β1 (5ffo) (*F*). One TGF-β monomer is colored blue, the other is colored green, and disulfides are shown as yellow sticks. (*G*) Comparison of integrin-binding loops from both Nb complex structures (green and blue) to the αVβ6-bound TGF-β1 monomer (orange) and the unbound TGF-β1 monomer (pink) after superposition on arm domains. Residues T256 and G276 in TGF-β2 are equivalent in sequence alignments to residues F239 and M253 in TGF-β1 and are shown as spheres.

by αVβ6 but not αVβ8. That mutation of just three amino acid residues to introduce the RGDLATI motif into TGF-β2 is sufficient to enable activation by αVβ8 shows that the integrin recognition motifs of the three TGF-βs are highly localized within their prodomains and exquisitely evolved to enable selective recognition by integrins of TGF-β isotypes.

αVβ6-mediated TGF-β1 activation is dependent on the β6 subunit cytoplasmic domain, which couples to the actin cytoskeleton, and occurs with TGF-β1 attached to a substrate and not with added recombinant TGF-β1 or cotransfected TGF-β1 lacking the Cys that links to milieu anchors, suggesting that it is force dependent (6, 20). Molecular dynamics simulations using the structure of αVβ6 bound to proTGF-β1 show that cytoskeletal-generated tensile force transmitted through the integrin and resisted by the TGF-β prodomain–milieu anchor complex results in unfolding of the prodomain straitjacket and release of the growth factor (18). We tested whether TGF-β2 activation is similarly dependent on the cytoplasmic domain of the β6 subunit. Putative binding sites for actin cytoskeleton adaptors talin and kindlin in NPLY and NVTY motifs were abolished with Tyr-to-Ala mutations in the $\beta6^{YY/AA}$ mutant. Similar mutations have been used to abolish talin/kindlin binding sites in the integrin β1 and β2 subunits (21–23). One or both motifs were also eliminated by truncating after residues 770 (770Δ) and 758 (758Δ) (Fig. 1*F*), which attenuated αVβ6 activation of TGF-β1 (6).

All three mutations similarly decreased activation of TGF-β2 and TGF-β1 (Fig. 1*F*). However, all three mutants retained residual ability to activate TGF-β compared to mock-transfected cells, suggesting a talin and kindlin cytoskeletal adaptor-independent component to αVβ6-dependent activation.

ProTGF-β2 Structures and Differences from TGF-β1. To obtain structural insight into TGF-β2 latency and activation by αVβ6, we cocrystallized TGF-β2 with nanobodies that we selected from a yeast display nanobody (Nb) library (24). A structure with Nb18 was refined to 2.2 Å, and a structure with Nb9 was refined to 3.15 Å that revealed the disulfide linkages in the bowtie (Fig. 2 and *SI Appendix*, Fig. S3 and Table S1). The two TGF-β2 structures are highly similar with a Cα RMSD of 0.71 Å, and the Nbs bind to similar sites on the prodomain shoulders. Although the prodomains of TGF-β2 and TGF-β1 are only 39% identical and have nine insertions and deletions (Fig. 2*A*), their procomplexes have similar overall conformations (Fig. 2 *B* and *C*).

The two prodomain arm domains are primarily formed from β-sheets that are disulfide-linked together at the "bowtie" knot (Fig. 2*B* and *SI Appendix*, Fig. S3*A*). Features stabilizing the extensive area of prodomain association with the growth factor (3200 $Å^2$) include hydrogen bonding between the β-sheets in the arm domain and growth factor and a prodomain straitjacket that encircles the growth factors composed of the α1-helix, latency lasso, α2-helix, and fastener.

Structural distinctions from TGF-β1 punctuate the TGF-β2 prodomain. A sequence insertion in TGF-β2 relative to TGF-β1 that follows the α2-helix correlates with a longer α2-helix in TGF-β2 (Fig. 2 *A*–*C*). A long meandering loop between the prodomain β1 strand and β2 strand (β1–β2 loop) is two residues longer in TGF-β2 than in TGF-β1 (Fig. 2 *A* and *B*). Whereas this loop is ordered in TGF-β1 (Fig. 2*C*), its much higher hydrogen–deuterium exchange in TGF-β2 (Fig. 2*A*) (19) suggests that it may be natively disordered. However, each Nb hydrogen bonds to and stabilizes formation of a "β*" strand in this loop. Binding of Nbs to this region may have contributed to crystallization; we were unable to obtain diffraction-quality crystals of TGF-β2 in their absence. The TGF-β2 bowtie has two reciprocal disulfides between Cys-226 and Cys-228 that are homologous to those in TGF-β1 and an additional Cys229–Cys229 disulfide; these disulfides link the two prodomain monomers (Fig. 2 *E* and *F* and *SI Appendix*, Fig. S3 *B*–*D*).

The bowtie tail, which contains the integrin binding site, is longer in TGF-β2 than in TGF-β1 and contains two disordered regions (Fig. 2*A*). The second disordered region contains the SGD sequence important for integrin-dependent activation followed by a highly basic sequence. The shorter bowtie tail of TGF-β1 (depicted in orange in Fig. 2*C*) contains the integrin-binding RGDLATI-motif; in the absence of integrin binding, its structure is variable or disordered in crystals (18, 25–27). Upon binding to TGF-β1, bowtie tail residues move as much as 17 Å to extend away from the body of the prodomain and position the RGDLATI motif for integrin binding (18) (Fig. 2 *C*, *Right* monomer, compared to the unbound monomer, Fig. 2 *C*, *Left* monomer).

Interestingly, the residues flanking the disordered αVβ6-binding site in TGF-β2 adopt the same conformation as seen in the αVβ6-bound conformation of TGF-β1 (Fig. 2*G*). This orientation suggests that the αVβ6-binding site in TGF-β2, although disordered, might be in a position favorable for integrin binding. The nanobodies do not appear to directly determine the position of the integrin-binding loop because it could take multiple alternative positions, including the location of the corresponding loop when unbound to integrin in TGF-β1 (Fig. 2 *C*, *Left*). However, the nanobodies do overlap with the position of the β1–β2 loop in TGF-β1, which they stabilize in TGF-β2 with formation of the β* strand. As the β1–β2 loop neighbors the integrin-binding loop, we cannot rule out an indirect effect of the nanobodies on the integrin-binding loop position.

Disulfides in ProTGF-β2 and Latency. Compared to TGF-β1, TGF-β2 has an additional prodomain cysteine, Cys-89, in the loop between the α2-helix and fastener that was disordered in both TGF-β2 Nb complex structures. To test for the presence of a C89-C89 disulfide bond, purified proTGF-β2 was digested with trypsin under native conditions and subjected to LC–tandem mass spectrometry. Fifteen spectral matches were observed for a disulfide-linked $AAAC^{89}ER$ peptide, demonstrating formation of the C89–C89 disulfide (*SI Appendix*, Fig. S4 *A*–*C*).

We next investigated how the four prodomain–prodomain disulfides in TGF-β2 contributed to prodomain dimerization and latency. After mutation to alanine of either all three bowtie cysteines or of the α2-helix–fastener loop cysteine, the prodomains remained largely dimeric (*SI Appendix*, Fig. S4*D*). However, the combined C89A+Bowtie quadruple mutant yielded predominantly the prodomain monomer in nonreducing SDS-PAGE. These results confirmed that structurally disordered Cys-89 forms an interchain disulfide even in the absence of disulfide bonds in the bowtie tail.

How important are these disulfide bonds in regulating TGF-β2 activation? The C89A mutation affected neither αVβ6-dependent nor independent TGF-β2 activity (Fig. 1*G*). The bowtie triple mutation led to a substantial increase of αVβ6-independent activation (Fig. 1*G*) but also retained considerable αVβ6-dependent activation. Although the C89A+bowtie quadruple mutant complex with GARP was expressed only half as well as WT, it showed increased αVβ6-independent activation and retained αVβ6-dependent activation. Furthermore, the comparison between the bowtie and C89A+bowtie mutations showed a contribution of the C89 disulfide to regulating αVβ6-independent activation. Overall, these results show that the C89 and bowtie disulfides cooperate to stabilize proTGF-β2 more against integrin-independent than against integrin αVβ6-dependent activation.

The Integrin αVβ6-Specific Recognition Sequence in TGF-β2. Previous comparisons of 9-mer prodomain peptides containing the RGD and SGD sequences from TGF-β1, β2, and β3 showed that the TGF-β2 peptide bound with substantially lower affinity to αVβ6 than TGF-β1 and β3 peptides (17). Using competition with a fluorescently labeled GRGDLGRLK TGF-β3 peptide, we confirmed the low affinity of αVβ6 for the TGF-β2 9-mer but found that proTGF-β2 bound with 170-fold higher affinity (Fig. 3 *A* and *B*). To test whether the recognition sequence was longer in TGF-β2 than in TGF-β1 and β3, we synthesized a 23-mer that encompassed the entire disordered SGD-containing loop revealed in TGF-β2 crystal structures. Indeed, the 23-mer bound αVβ6 with an affinity 20-fold higher than the 9-mer and only eightfold lower than intact proTGF-β2. To find the minimal recognition sequence, we truncated one or two residues at a time from the N or C termini of the 23-mer peptide and defined clear endpoints at each terminus (*SI Appendix*, Fig. S5 *A*, *B*, and *D*). The minimal peptide of 13 residues, $Y^{259}TSGDQKTIKSTR^{271}$, bound to αVβ6 with identical affinity as the 23-mer (Fig. 3 *A* and *B*). Compared to αVβ6, αVβ8 bound the 23-mer and 13-mer peptides with 5,500 to 8,100-fold lower affinity, with K_D's of 7.7 and 11.4 mM (*SI Appendix*, Fig. S5*C*). Substitutions in the 13-mer tested the importance of each residue for αVβ6 binding (Fig. 3 *B*–*D*). Ala substitutions of G262, D263, and I267 resulted in the most severe reductions in affinity, while Ala substitutions of S261, Q264, K268, and R271 led to more moderate decreases

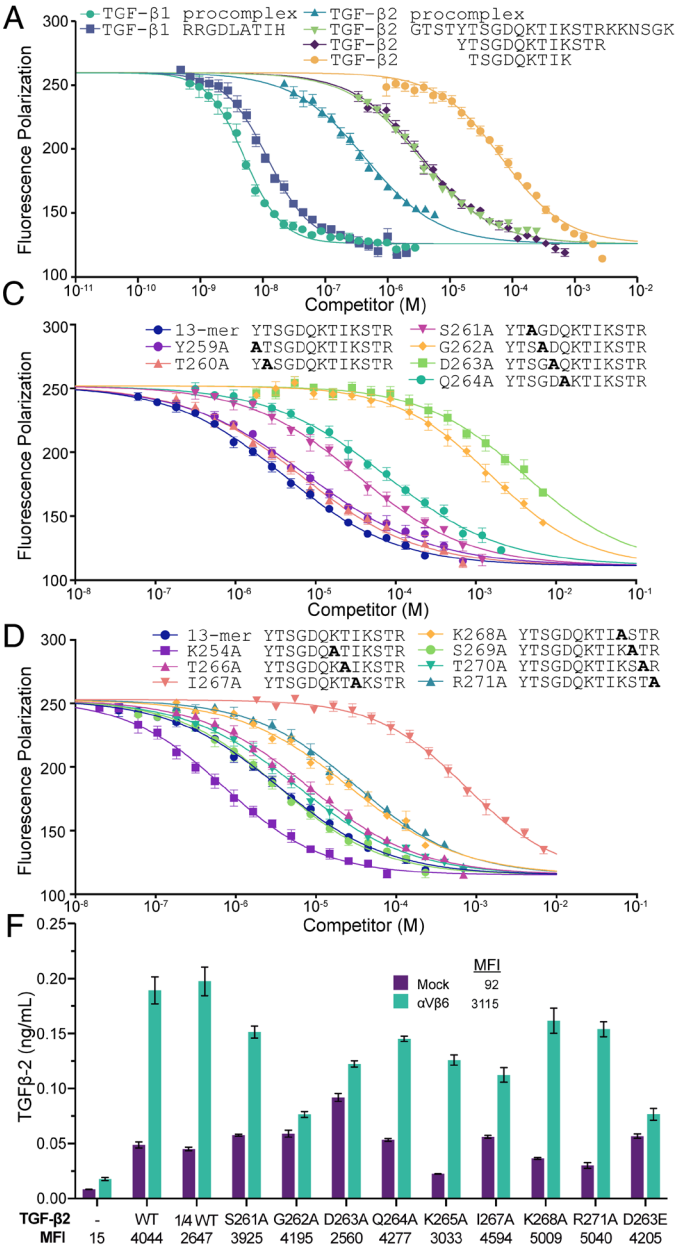

B Unclasped αVβ6 ectodomain affinity

Competitor	K_D (μM) [a]	Fold [b]
ProTGF-β1	0.0049 ± 0.0015	1.0
• RRGDLATIH	0.0070 ± 0.0019	1.4
ProTGF-β2	0.170 ± 0.016	1.0
• 23-mer (GTSTYTSGDQKTIKSTRKKNSGK)	1.4 ± 0.1	8.2
• 13-mer (YTSGDQKTIKSTR)	1.4 ± 0.3	8.2
• 9-mer (TSGDQKTIK)	29.1 ± 2.6	171.1
• 13-mer (YTSGDQKTIKSTR)	1.5 ± 0.2	1.0
• Y259A (ATSGDQKTIKSTR)	3.2 ± 0.5	2.1
• T260A (YASGDQKTIKSTR)	2.7 ± 0.4	1.8
• S261A (YTADQKTIKSTR)	14.0 ± 2.2	9.3
• G262A (YTSADQKTIKSTR)	610 ± 97	406.7
• D263A (YTSGAQKTIKSTR)	1400 ± 240	933.3
• Q264A (YTSGDAKTIKSTR)	32 ± 5	21.3
• K265A (YTSGDQATIKSTR)	0.25 ± 0.04	0.17
• T266A (YTSGDQKAIKSTR)	3.0 ± 0.5	2.0
• I267A (YTSGDQKTAKSTR)	271 ± 42	180.7
• K268A (YTSGDQKTIASTR)	9.4 ± 1.4	6.3
• S269A (YTSGDQKTIKATR)	1.3 ± 0.2	0.9
• T270A (YTSGDQKTIKSAR)	2.2 ± 0.3	1.5
• R271A (YTSGDQKTIKSTA)	12 ± 2	8.0

[a] Values are ± fitting errors.
[b] Fold change comparisons are within the same experiments enclosed by brackets.

Fig. 3. Defining the integrin αVβ6 binding site in TGF-β2. (*A–D*) Affinity measurements with fluorescence polarization (FP). TGF-β1 and TGF-β2 proteins and peptides were used to compete binding of 10 nM FITC-TGF-β3 GRGDLGRLK peptide to 20 nM αVβ6 ectodomain. Data in panels (*A*, *C*, and *D*) are mean ± SE of three independent experiments [five for the 13-mer peptide in panels (*C* and *D*)] each performed in duplicate and were fitted to a variable slope (four-parameter) dose–response curve. (*A*) Comparison of intact TGF-β1 and TGF-β2 to peptides. (*B*) Summary table of K_D's measured in this study. Fold change comparisons are enclosed in brackets and are relative to proTGF-β1, proTGF-β2, or the TGF-β2 13-mer peptide as indicated. (*C* and *D*) TGF-β2 13-mer peptides with Ala mutations. Panels (*C* and *D*) display the same data for the wild-type 13-mer. (*E*) Inhibition of αVβ6-mediated activation of TGF-β2 by the K265A 13-mer TGF-β2 peptide compared to the 9-mer TGF-β1 peptide and the αVβ6 antibody 7.1g10. Data were fit to a four-parameter dose–response curve to calculate IC_{50} values. (*F*) Effect of mutations in the integrin αVβ6 binding motif in TGF-β2 on activation. Expi293 GARP/TGF-β2 cotransfectants were cocultured with mock or αVβ6 Expi293 transfectants and CAGA-reporter cells. Data are mean SD of three technical replicates from a representative experiment. Overall data from three independent experiments are reported in *SI Appendix*, Fig. S5*E*. To control for mutants with lower expression, WT GARP/TGF-β2 cotransfection with 1/4 amount of plasmid was included. MFI for cell surface integrins and FLAG-tagged TGF-β2 constructs are reported in the key and below the graph, respectively. (*G*) Correlation of TGF-β2 mutant peptide affinity (*B*) with the effect of the corresponding mutation in TGF-β2/GARP complexes on integrin αVβ6-dependent activation (activation with αVβ6 transfectants–activation with mock transfectants in *F*).

in affinity. Intriguingly, the K265A mutation yielded a 6.3-fold increase in affinity for αVβ6.

Biological relevance of the peptide results was tested in assays of TGF-β2 activation. The 13-mer TGF-β2 K265A peptide was able to inhibit αVβ6-dependent TGF-β2 activation with a potency relative to the 9-mer TGF-β1 peptide (Fig. 3*E*) that was similar to their relative affinities for αVβ6 (Fig. 3*B*). Furthermore, Ala substitutions that affected 13-mer peptide affinity for αVβ6 were incorporated into intact TGF-β2 and assayed for their effects on activation of TGF-β2 from GARP complexes. αVβ6-dependent activation of TGF-β2 was little affected by Ala substitutions that moderately decreased peptide affinity or increased affinity but was strongly inhibited by the mutations with the strongest effects on affinity, i.e. G262A, D263A, and I267A, as well as the SGE (D263E) mutation (Fig. 3 *F* and *G*). In summary, we mapped the αVβ6 recognition sequence in TGF-β2 to a 13-residue peptide

that is located within a disordered loop that is well exposed for αVβ6 binding, and its biological relevance was established in assays of αVβ6-dependent TGF-β2 activation.

Discussion

It has been widely assumed that RGD-binding integrins do not activate TGF-β2 because it lacks an RGD motif (4, 28–30). Furthermore, although a previous study reported that integrin αVβ6 was unable to activate latent TGF-β2 (7), TGF-β2 was not cotransfected with a milieu anchor, which we show here is important for robust αVβ6-dependent activation of TGF-β2. A recent paper that examined the contributions of TGF-β1, β2, and β3 to fibrosis demonstrated αVβ6-dependent activation of TGF-β1 and β3 but did not test αVβ6 dependence of TGF-β2 activation (4). Our unexpected observation of αVβ6-dependent activation of TGF-β2 overturns dogma, has significant biological implications, and illustrates yet again the importance of milieu anchors in TGF-β biology (31).

All TGF-βs have a cysteine near their N terminus that links to a milieu anchor, with which association is required for secretion and biological function (11, 13, 31–33). In the absence of cotransfection with a milieu anchor, the presence or identity of a milieu anchor in the transfected cell is unknown. For comparison to previous literature, we compared TGF-β transfection in the presence and absence of milieu anchors and found differences in how milieu anchors regulated TGF-β1, β2, and β3 activation. Robust integrin αVβ6 activation of TGF-β2 required cotransfection with a milieu anchor. Integrin αVβ6- and αVβ8-mediated activation of TGF-β1 occurred in the absence of and was enhanced in the presence of milieu anchors. Integrin-independent activation was particularly marked for TGF-β3 both in the presence and absence of cotransfection with milieu anchors, in agreement with a study that omitted cotransfection with milieu anchors (4). The greater importance of milieu molecule cotransfection for integrin-mediated TGF-β2 activation might be i) because cells commonly used for transfection natively express a milieu anchor that interacts better with TGF-β1 and β3 than TGF-β2 or ii) because the presence of the unsatisfied hydrophobic interface and cysteine in the milieu-anchor binding interface in TGF-βs is more disruptive to folding and expression in TGF-β2 than in TGF-β1 and β3.

Among the 24 integrins in mammals, the 8 RGD-binding integrins are unusual in their ability to recognize motifs that are natively disordered. Recognition of RGD motifs is often accompanied by promiscuity; however, when combined with recognition of neighboring ordered synergistic sites, selectivity can be achieved (34). Remarkably, for integrins αVβ6 and αVβ8 to achieve selectivity, binding to the poorly ordered RGDLXX (L/I) motif is sufficient, as shown by structural analysis and similar affinities of peptides and proTGF-β1 (17, 18, 35, 36).

Starting with the 23-residue peptide encompassing the disordered bowtie tail of proTGF-β2, we identified the shortest fragment that retained full affinity for αVβ6. This 13-residue peptide bound to αVβ6 with only slightly lower affinity than proTGF-β2 and competed binding of a proTGF-β3 peptide, suggesting that αVβ6 recognition of proTGF-β1, β3, and β2 is similarly focused on natively disordered peptide segments within the prodomain bowtie tail with little contribution from other regions. Although the bowtie tail has two or more distinctive poses within proTGF-β1, with non-integrin binding poses dominant in the absence of integrin binding (18), our structures of TGF-β2 suggest that TGF-β2 might have a single pose that corresponds to the integrin-binding pose of proTGF-β1.

Our study revealed a 13-residue YTSGDQKTIKSTR motif in TGF-β2 that is recognized only by integrin αVβ6 and diverges from the seven-residue RGDLXX (L/I) motif in TGF-β1 and TGF-β3 that is recognized by both αVβ6 and αVβ8. The last four residues of RGDLXX (L/I) form an amphipathic α-helix that nestles its hydrophobic face in a binding pocket in the β6 or β8 subunits (17, 18, 35, 36). The peptide in TGF-β2 must bind differently because more N- and C-terminal residues were required for maximal binding affinity than in TGF-β1 (17) and because of other differences including the lack of the Arg of RGD and the importance of Gln rather than the Leu following the RGD motif that makes an important contribution to binding of the amphipathic helix in TGF-β1 (18). Future structural studies will be important to determine how the YTSGDQKTIKSTR motif binds to αVβ6 to create the exquisite specificity of TGF-β2 for αVβ6 compared to αVβ8 and other integrins.

Although a family of 33 homologous cytokines in vertebrates is named after TGF-β and are found in the most primitive metazoans, TGF-βs appear much later in evolutionary history, in deuterostomes. Representatives of the early deuterostome phyla Echinodermata and Hemichordata, and early Chordata including tunicates and lancelets, encode only one TGF-β that in each case possesses an RGD-motif (Fig. 4). In contrast, jawed vertebrates encode three TGF-β paralogs with RGD motifs in TGF-β1 and β3 and SGD, AGD, or GGD motifs in TGF-β2. In agreement, our peptide substitutions show little effect on affinity for αVβ6 of changing SGD to AGD. Like the three TGF-βs, the integrin β6 and β8 subunits also first appeared in vertebrates. Thus, loss of the RGD motif in TGF-β2 and its modification for selective activation by αVβ6 is a trait acquired in vertebrates.

All of our assays showed αVβ6-independent, as well as dependent, mechanisms of TGF-β2 activation. αVβ6-deficient mice (*Itgb6*$^{-/-}$) exhibit lung and skin inflammation (38) and do not phenocopy the developmental defects and perinatal lethality observed in *Tgfb2*$^{-/-}$ mice (1). This discrepancy supports the physiologic importance of αVβ6-independent TGF-β2 activation. While proteolysis has been proposed as a TGF-β2 activation mechanism (30, 39, 40), more characterization of integrin-independent mechanisms of TGF-β activation is required. Compared to TGF-β2, we found smaller and more substantial amounts of integrin-independent activation of TGF-β1 and TGF-β3 (4), respectively.

The previously unappreciated ability of integrin αVβ6 to activate TGF-β2 has important implications for therapy of fibrosis with αVβ6 inhibitors. Integrin αVβ6 mediates fibrosis in multiple tissues including the lung, liver, and kidney (41), and TGF-β2 drives lung and hepatic fibrosis (4). After lung injury, type 2 alveolar epithelial cells facilitate the repair and regeneration of damaged lung epithelia. TGF-β halts type 2 alveolar epithelial cell proliferation during tissue repair, and scRNAseq showed that upregulation of the integrin αV and β6 subunits and TGF-β2, and not TGF-β1 or TGF-β3, coincided with the halt of alveolar epithelial cell proliferation (42). TGF-β is an important tumor suppressor of normal and premalignant epithelial cell types (43). Integrin αVβ6 is primarily expressed in epithelial cells, and its deficiency in mice results in dysregulation in the lungs and skin (38) and a significant incidence of carcinomas (44). A small-molecule inhibitor of αVβ6 was recently found to induce on-target epithelial cell proliferation and invasive uroepithelial carcinoma in rhesus macaques (45); small-molecule inhibitors of TGFβR1 cause similar cancers. Idiopathic pulmonary fibrosis clinical trials of an inhibitory antibody to αVβ6 were stopped for safety concerns (46). Previously, it was thought that integrins activated only TGF-β1 and β3. The identification here of a motif in proTGF-β2 for integrin αVβ6-dependent activation makes it important to determine the role of αVβ6 in TGF-β2 activation in vivo and to take such activation into account in the development of safe and efficacious integrin αVβ6 therapeutics.

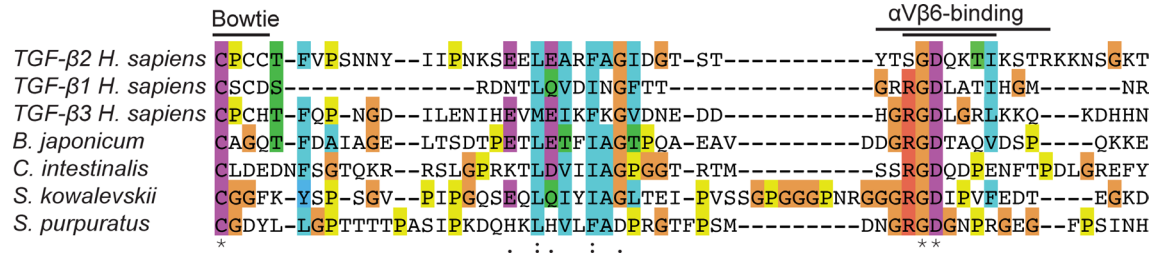

Fig. 4. Bowtie and bowtie tail sequences of TGF-βs. Full-length TGF-β sequences were aligned with MAFFT (37); the portion between the β7 and β10 strands (Fig. 2*A*) is shown. The three human TGF-βs (Chordata, Vertebrata; all from RefSeq) were aligned with the sole TGF-β's from *Branchiostoma japonicum* (Chordata, Cephalochordata; UniProt: F6M2M4), *Ciona intestinalis* (Chordata, Tunicata; UniProt: Q4H2P5), *Saccoglossus kowalevskii* (Hemichordata; UniProt: A0A0U2L5S7), and *Strongylocentrotus purpuratus* (Echinodermata; UniProt: A0A7M7RFG3). The αVβ6-binding motifs are indicated for TGF-β2 (*Top* line) and for TGF-β1 and TGF-β3 (*Lower* line).

Materials and Methods

Methods.

Cell lines and culture. Expi293F cells were cultured in suspension using a 1:1 mix of FreeStyle293 and Expi293 growth medium at 37 °C, 8% CO_2. HEK293 cells transfected with a luciferase construct under control of the CAGA element (CAGA reporter cells) (9) were provided by T. Thompson (University of Cincinnati) and cultured as adherent cells in Dulbecco's modified Eagles medium containing 10% fetal bovine serum and 100 μg/mL G418 at 37 °C, 7.5% CO_2.

Coculture TGF-β activation assay. N-terminally FLAG-tagged human TGF-β1, TGF-β2 (wild-type and mutant constructs), and TGF-β3, and full-length human GARP with an N-terminal SNAP-tag are in the pLEXm mammalian expression vector (47). Full-length human LTBP-1S is in a modified pIRES2-EGFP vector (BD Biosciences, San Diego, CA), which contains a streptavidin-binding peptide tag at the C terminus (13), whereas LTBP-3 is in pcDNA3 and was a kind gift from Daniel Rifkin (NYU Grossman School of Medicine) (7). pcDNA3.1-alpha4 wt (Hygro) (human integrin α4) was Addgene plasmid # 80017 (48). Human integrins αV, α5, α8, and αIIb were in pD2529-CAG (ATUM). Human integrins β1, β3, β5, β6 (wild-type and mutant constructs) and β8 in pD2529-CAG (ATUM) were C-terminally fused to a p2A skip peptide (49) followed by mCherry to visually monitor transfection efficiency. pLEXm and pD2529-CAG were used as empty vector controls in mock transfections.

All transfections were performed in 6-well tissue culture plates, and coculture TGF-β activation assays were performed in 96-well flat-bottom tissue culture plates. Expi293 cells were seeded in 6-well plates (8×10^5 cells/well) in FreeStyle293 media 24 h prior to transfection using jetPRIME reagent (Polyplus, Illkirch-Graffenstaden, France). For each transfection, 3.2 μg total DNA was diluted in 320 μL of jetPRIME buffer, vortexed, and spun. In addition, 6.4 μL of the jetPRIME transection reagent was added to the DNA mixture, vortexed, and incubated for 10 min at room temperature before being added dropwise to the seeded Expi293 cells. For TGF-β transfectants, 1.6 μg TGF-β constructs were cotransfected with 1.6 μg of a milieu anchor construct or pLEXm, except experiments in Fig. 1*G* used 0.4 μg GARP, 0.4 μg TGF-β2 (WT, C89A, or bowtie mutants) and 2.4 μg pLEXm to enable comparisons to lower cell surface expression of the C89A+bowtie mutant. In addition, 1.6 μg pLEXm and 1.6 μg milieu anchor constructs were cotransfected for mock TGF-β. For integrin transfectants, 1.6 μg of each integrin α and β subunit was cotransfected, and 3.2 μg pD2529 was used for mock integrin transfections. Transfectants were cultured at 37 °C and 7.5% CO_2.

Subsequently, 48 h after transfection, CAGA reporter cells and transfectants were resuspended in fresh FreeStyle293 media for coculture activation assays. CAGA reporter cells (15,000 cells) were cocultured with TGF-β or milieu anchor/TGF-β transfectants (2,500 to 5,000 cells) and with pD2529 (mock) or integrin transfectants (15,000 cells) in 96-well plates for 24 h at 37 °C and 7.5% CO_2. Additional pLEXm (mock TGF-β) transfectants were added to reach a final count of 45,000 cells/well. All coculture assays used 5,000 TGF-β or milieu anchor/TGF-β transfectants except for the experiment in Fig. 1*G*, which was adjusted to 2,500 cells to ensure that luciferase activity of activating mutants was still in the range of the standard curve. For experiments testing inhibition of TGF-β activation by the αVβ6-function blocking antibody 7.1g10 or TGF-β peptides, serial two-fold dilutions in FreeStyle293 media were added to CAGA reporter cells mixed with TGF-β or milieu anchor/TGF-β transfectants followed by addition of integrin transfectants. For standard curves, recombinant human TGF-β1 (Sigma cat. # T7039) or TGF-β2 (Sigma cat. # H8666) growth factor at 20 ng/mL and serial two-fold dilutions thereof in FreeStyle293 media were added to 15,000 CAGA reporter cells cocultured with 30,000 mock transfectants. Then, 16 h after coculture or incubation with recombinant growth factor, TGF-β-induced luciferase activity was measured using the Promega Luciferase Assay System (*Cat. No. E1501)* on a BioTek Synergy H1 Spectrophotometer. For assays testing inhibition of TGF-β2 activation by TGF-β2-derived peptides, luciferase activity was measured after 8 h of coculture. Standard curve interpolation of raw luciferase values and statistical analyses including two-way ANOVA and Tukey's multiple comparison testing were performed using Prism 9.4.1.

Flow cytometry. All washes and antibody incubations were performed in FACS buffer (Hanks Balanced Salt Solution, 1 mM $MgCl_2$, 1 mM $CaCl_2$, and 1% BSA). Expi293F cell transfectants were washed once prior to antibody staining. Integrin transfectants were incubated with 20 μg/mL of mouse anti-human αV (17E6) (50), mouse anti-human αVβ6 (7.1g10) (15), rat anti-human β1 (mAb13) (51), mouse anti-human β3 (7E3) (52), rat anti-human α5 (51), or humanized anti-human α4 (53) directly labeled with AlexaFluor647 (Natalizumab-AF647) in 96-well plates for 1 h on ice. For secondary detection of 17E6, 7.1g10, mAb13, and 7E3 staining, transfectants were washed twice and incubated for 30 min with 20 μg/mL of AlexaFluor-647 labeled goat anti-mouse IgG (Thermofisher cat. # A-21235) or AlexaFluor-647 labeled chicken anti-rat IgG (Thermofisher cat. #A-21472) at 4 °C. Expi293F cells cotransfected with Flag-tagged TGF-βs and GARP were stained with the APC anti-DYKDDDDK tag (clone L5, BioLegend) at 2 μg/mL for 30 min on ice. After two additional washes with FACS buffer, stained cells were resuspended in 400 μL of FACS buffer, transferred to 5 mL polystyrene round-bottom tubes, and analyzed by flow cytometry using FACS Canto II (BD Biosciences). Voltages and gates were set for each antibody using a mock transfectant stained with the corresponding antibody.

Nb Selection and Expression. First, 5×10^9 *S. cerevisiae* cells expressing a surface-display library of single-domain camelid antibody VHH domains Nb (24) were centrifuged, resuspended in binding buffer (phosphate-buffered saline, 0.1% BSA), and incubated with anti-biotin-coated magnetic microbeads (Miltenyi) for 1 h at 4 °C. Then, the yeast were passed through two autoMACS columns in series using the Possel function in an autoMACS Pro Separator (Miltenyi) to deplete the library of yeast expressing nanobodies that bind to the microbeads or anti-biotin. The autoMACS flowthrough containing the depleted library was then centrifuged, resuspended in binding buffer, and incubated with 500 nM chemically biotinylated proTGF-β2 for 1 h at 4 °C. The yeast were then centrifuged, resuspended in binding buffer, and incubated with anti-biotin-coated microbeads (Miltenyi) for 20 min at 4 °C before being passed through two autoMACS columns in series using the Possel function. The eluate containing yeast expressing proTGF-β2-binding nanobodies was collected, expanded, and used in subsequent rounds.

Three positive affinity FACS steps interspersed with two negative FACS steps were used for further Nb selection. The positive sorts were performed with progressively decreasing concentrations of biotinylated proTGF-β2 starting at 200 nM, then 50 nM, and finally 16 nM to positively enrich for high-affinity Nbs. AF488-antiHA (Cell Signaling Technology) was used for detection of Nb display on the yeast surface. The 200 nM and 16 nM steps used streptavidin-APC (Tonbo, San Diego, CA) to detect binding of biotinylated proTGF-β2, whereas the 50 nM step used streptavidin-PE (Invitrogen cat. # S866). For the interspersed negative selection steps to remove nonspecific and polyreactive clones, we sorted

for cells that did not react in FACS with a polyreactivity reagent consisting of a biotinylated preparation of baculovirus-infected Sf9 membrane proteins (54). Polyreactivity reagent binding was detected using streptavidin-APC in the first negative sort and streptavidin-PE in the second negative sort, thus also removing nonspecific binders to both secondary detection reagents. After FACS selections, we isolated 48 yeast clones and identified eight unique Nb sequences through Sanger sequencing.

Protein expression and purification. The sequence of the human proTGF-β2 construct was as follows:

MKWVTFLLLLFISGSAFSGSH HHH HHH HLSTGG SDE KTT GWR GGH VVE GLAGELEQLRARLEH HPQGQREPGSGLEVLFQGPSLSTS$^{(C24S)}$ STLDMDQ FMRKRIEAIRGQILSKLKLTSPPEDYPEPEEVPPE VISIYNSTRDLLQ EKASRRA AAC ERE RSD EEY YAK EVY KID MPP FFP SENAIPPTFYRPYF RIVRFDVSA MEKR$^{(N140R)}$ASNLVKAEFRVFR LQNPKARVPEQRIELYQILKSKDLTSPTQR Y IDSKVVKTRAEGEWLSFDVTDAVHEWLHHKDRNLGFKISLHCPCCTFVPSN NYIIPNKSEELEARFAGIDGTSTYTSGDQKTIKSTRKKNSGKTPHLLLMLLPSYRLE SQQTNG$^{(R298_R303delinsG)}$ ALDAAYCFRNVQDNCCLRPLYIDFKRDLGWKW IHEPKGYNANFCAGACPYLWSSDTQHSRVLSLYNTINPEASASPCCVSQDLE PLTILYYIGKTPKIEQLSNMIVKSCKCS

The construct contains the signal peptide from rat serum albumin (MKWVTFLLLLFISGSAFS), a GS linker, followed by N-terminal 8-His tag, a Streptavidin-Binding Peptide (SBP) tag, and a 3C protease site (all underlined). In bold are mutations that were introduced to facilitate expression, secretion, and crystallization. Numbering is based on immature TGF-β2. C24S removes the Cys that links to milieu anchors; N140R removes an N-glycosylation site; and replacement of residues 298 to 302 (RRKKR) with a single Gly (D5G) removes the PC cleavage site and shortens its loop. The proTGF-β2 construct was cloned into the pEF1-puro vector (55) and stably expressed in GnTI-deficient HEK293S cells (56) to obtain high-mannose glycoforms. ProTGF-β2 protein was purified in three steps as described (19). High-mannose proTGF-β2 was then "shaved" with EndoH (NEB, Ipswich, MA USA) for removal of high-mannose glycans to facilitate crystallization. Shaved proTGF-β2 and EndoH were separated by size-exclusion chromatography over a Superdex 200 column in 20 mM Tris, pH 8.0, 150 mM NaCl. The purified shaved proTGF-β2 was concentrated to 14.8 mg mL^{-1} in 20 mM Tris, pH 8.0, 150 mM NaCl and used for crystallization and fluorescence polarization (FP) assays.

Nb9 and Nb18 were cloned into the pET26b vector in frame with a C-terminal 6× His tag for periplasmic expression in BL21 (DE3) *E. coli*. Transformed BL21 (DE3) cells were induced with IPTG to express each Nb clone and subjected to osmotic shock to release periplasmic Nb (24). The His-tagged nanobodies were purified over Ni-NTA agarose, washed with 20 mM HEPES, pH 7.5, 500 mM NaCl, and 20 mM imidazole, then washed with 20 mM HEPES, pH 7.5, 100 mM NaCl, and 20 mM imidazole, and eluted with 20 mM HEPES, pH 7.5, 100 mM NaCl, and 400 mM imidazole. Nanobodies were dialyzed in 20 mM HEPES, pH 7.5, 500 mM NaCl, and 0.5 mM EDTA and purified by size chromatography over a Superdex 75 column in the same buffer. Nbs 9 and 18 were concentrated to 3.7 and 9.2 mg mL^{-1}, respectively.

Crystal structures. For crystallization, shaved proTGF-β2 C24S, N140R, D5G (in 20 mM Tris pH 8.0, 150 mM NaCl) was mixed with Nb9 (in 20 mM HEPES, pH 7.5, 500 mM NaCl, 0.5 mM EDTA) or Nb18 (in 20 mM HEPES, pH 7.5, 500 mM NaCl, 0.5 mM EDTA) at a 1:1 monomer molar ratio to final total protein concentrations of 10 mg/mL or 2.5 mg/mL, respectively. Crystals of the Nb9/proTGF-β2 complex (1 μL) were formed in hanging drops at 20 °C with 1 μL of 100 mM HEPES, pH 7.6, 10% PEG 4,000. For cryoprotection, 1 μL of 30% glycerol in well solution was added to the hanging drop (~15% glycerol). Crystals were harvested in cryoloops, briefly submerged in 30% glycerol in well solution, and flash-frozen in liquid nitrogen.

Crystals of the Nb18/proTGF-β2 complex (1 μL) were formed in hanging drops at 20 °C with 1 μL of 100 mM HEPES, pH 7.4, and 26.7% Jeffamine ED2001. For cryoprotection, 1 μL of 30% glycerol in 100 mM HEPES, pH 7.2, and 25% Jeffamine ED2001 was added to the hanging drop (~15% glycerol). Crystals were then harvested in cryoloops, briefly submerged in 30% glycerol in 100 mM HEPES, pH 7.2, and 25% Jeffamine ED2001, and flash-frozen in liquid nitrogen. Diffraction data were collected using beamline 17-ID-1 (AMX) of the National Synchrotron Light Source II for Nb9/proTGF-β2 and the GM/CA beamline 23-IDD at the Advanced Photon Source for Nb18/proTGF-β2. Software used in this project was curated by SBGrid (57). XDSGUI was used for diffraction data processing (58). AIMLESS and POINTLESS in CCP4 were used for scaling, merging, and point group determination (59, 60). The Nb9/proTGF-β2 complex structure was solved using the TGF-β1 prodomain (PDB 5VQP) (26), the TGF-β2 growth factor (PDB 2TGI) (61), and Nb.b201 (PDB 5VNV) (24) as search models for molecular replacement with Phaser (62). The Nb18/proTGF-β2 complex structure was solved using molecular replacement with Nb9 and a proTGF-β2 monomer from the Nb9/proTGF-β2 complex structure as search models in Phaser. Autobuilding was performed using Phenix followed by iterative rounds of model building in Coot and refinement in Phenix (63–65). MolProbity was used to guide rebuilding and in the final calculation of Ramachandran, clash, and geometry statistics (66).

Liquid chromatography and tandem mass spectrometry. ProTGF-β2 was resuspended in 200 mM 4- (2-hydroxyethyl)-1-piperazinepropanesulfonic acid (EPPS), pH 8.5, and digested at 37 °C for 6 h with trypsin at a 100:1 protein-to-protease ratio. Mass spectrometric data were collected on an Orbitrap Exploris 480 mass spectrometer (ThermoFisher Scientific, San Jose, CA) coupled to a Proxeon EASY-nLC 1,200 liquid chromatograph (ThermoFisher Scientific, San Jose, CA). Peptides were separated on a 100 μm inner diameter microcapillary column packed with ~35 cm of Accucore150 resin (2.6 μm, 150 Å, ThermoFisher Scientific, San Jose, CA). We loaded 2 μg onto the column, and separation was achieved using a 75-min gradient of 7 to 27% acetonitrile in 0.125% formic acid at a flow rate of ~600 nL/min. Mass spectrometric data were collected using the high-resolution MS2 (hrMS2) method. The scan sequence began with an MS1 spectrum (Orbitrap analysis; resolution, 120,000, mass range, 350 to 1,200 Th; automatic gain control (AGC) target 300%; maximum injection time, auto). MS2 spectra were acquired for the top 20 most abundant features via high energy collision-induced dissociation with the following settings: resolution, 30,000; AGC target, standard; isolation width, 1.2 Th; normalized collision energy (%), 28; maximum injection time, 60 ms. Mass spectra were processed and searched using the PIXL search engine [Mintseris & Gygi, PNAS 117 (1) 93 to 102], setting precursor tolerance to 15 ppm and fragment ion tolerance to 10 ppm. Methionine oxidation was set as a variable modification, and cross-linker mass shift was set to −2.01565. PIXL searches included 50 most abundant protein sequences to ensure sufficient statistics, and matches were filtered to a 1% false-discovery rate.

FP-based competitive binding assays and peptides. αVβ6 or αVβ8 ectodomain was preequilibrated with the FITC-labeled TGF-β3 peptide (GRGDLGRLK) for 1 h on ice before being mixed with serial dilutions of TGF-β proteins or peptides in flat-bottomed black 384-well plates (Corning). Each 10-μL sample contained 20 nM αVβ6 ectodomain or 200 nM αVβ8 ectodomain, 10 nM FITC-labeled TGF-β3 peptide, and the indicated protein or peptide in 20 mM Tris buffer (pH 7.4), 150 mM NaCl, 1 mM $CaCl_2$, and 1 mM $MgCl_2$. GenScript (Piscataway, New Jersey USA) synthesized all the peptide competitors used in this study with N-terminal acetylation and C-terminal amidation. Peptides were resuspended in water at 50 mM stock concentration. For FP assays, peptides were diluted in 20 mM Tris buffer (pH 7.4), 150 mM NaCl, 1 mM $CaCl_2$, and 1 mM $MgCl_2$ to starting concentrations ranging from 2 to 6933 μM. ProTGF-β1 and proTGF-β2 at starting concentrations of 1.4 and 46 μM, respectively, were diluted in the same buffer. Serial 1.41-fold and 1.73-fold dilutions were carried out for 24-point assays and 16-point assays, respectively. The mixtures were equilibrated for one hour on ice before measuring FP using a Synergy Neo plate reader (BioTek). Pilot measurements at 1, 2, and 4 h showed negligible differences and indicated that 1 h incubation was sufficient for binding to reach equilibrium. Experiments consisted of duplicate measurements and were performed at least three times. K_D values were determined as previously described (67).

Data, Materials, and Software Availability. Atomic coordinates and structure factors data have been deposited in the Protein Data Bank (PDB) under accession codes 8FXS (68) and 8FXV (69). All study data are included in the article and/or *SI Appendix*.

ACKNOWLEDGMENTS. We would like to thank Amir Khan and Jordan Anderson for help with crystallography, data collection, and data processing; SBGRID for structural biology software and data processing support; Aravind Ramakrishnan for helpful discussions; Jing Li for help with fluorescence polarization assays, data fitting, and reagents; Yuxin Hao for reagents; and Margaret Nielsen for her assistance in designing figures. GM/CA beamline 23ID-D was funded by the NCI (ACB-12002) and the NIGMS (AGM-12006, P30GM138396). This research used

beamline 17-ID-1 of the Advanced Photon Source, a US Department of Energy (DOE) Office of Science User Facility operated for the DOE Office of Science by Argonne National Laboratory under Contract No. DE-AC02-06CH11357. The Center for BioMolecular Structure is primarily supported by the NIH, National Institute of General Medical Sciences (NIGMS) through a Center Core P30 Grant (P30GM133893), and by the DOE Office of Biological and Environmental Research (KP1605010), at the National Synchrotron Light Source II, a US Department of Energy Office of Science User Facility operated for the DOE Office of Science by Brookhaven National Laboratory under Contract No. DE-SC0012704. This study was funded by NIH grant R01-HL-159714 (T.A.S.), NIH grant T32-DK-007527 (V.Q.L.), NIH grant K01-DK124443 (V.Q.L.), National Natural Science Foundation of China No. 31971145 (B.Z.), and 2022–2023 Peter Morgane Student Research Fellowship (C.T.).

Author affiliations: [a]Program in Cellular and Molecular Medicine, Department of Pediatrics, Boston Children's Hospital, Boston, MA 02115; [b]Department of Biological Chemistry and Molecular Pharmacology, Harvard Medical School, Boston, MA 02115; and [c]Department of Cell Biology, Harvard Medical School, Boston, MA 02115

1. L. P. Sanford *et al.*, TGFβ2 knockout mice have multiple developmental defects that are non-overlapping with other TGFβ knockout phenotypes. *Development* **124**, 2659–2670 (1997).
2. T. Doetschman *et al.*, Transforming growth factor β signaling in adult cardiovascular diseases and repair. *Cell Tissue Res.* **347**, 203–223 (2012).
3. M. Morikawa, R. Derynck, K. Miyazono, TGF-β and the TGF-β family: Context-dependent roles in cell and tissue physiology. *Cold Spring Harb. Perspect. Biol.* **8**, a021873 (2016).
4. T. Sun *et al.*, TGFβ2 and TGFβ3 isoforms drive fibrotic disease pathogenesis. *Sci. Transl. Med.* **13**, eabe0407 (2021).
5. A. P. Hinck, T. D. Mueller, T. A. Springer, Structural biology and evolution of the TGF-β family. *Cold Spring Harb. Perspect. Biol.* **8**, a022103 (2016).
6. J. S. Munger *et al.*, The integrin αvβ6 binds and activates latent TGFβ1: A mechanism for regulating pulmonary inflammation and fibrosis. *Cell* **96**, 319–328 (1999).
7. J. P. Annes, D. B. Rifkin, J. S. Munger, The integrin αvβ6 binds and activates latent TGFβ3. *FEBS Lett.* **511**, 65–68 (2002).
8. D. Mu *et al.*, The integrin αVβ8 mediates epithelial homeostasis through MT1-MMP-dependent activation of TGF-β1. *J. Cell Biol.* **157**, 493–507 (2002).
9. J. N. Cash *et al.*, Structure of myostatin.follistatin-like 3: N-terminal domains of follistatin-type molecules exhibit alternate modes of binding. *J. Biol. Chem.* **287**, 1043–1053 (2012).
10. A. Jiang, Y. Qin, T. A. Springer, Loss of LRRC33-dependent TGFβ1 activation enhances antitumor immunity and checkpoint blockade therapy. *Cancer Immunol. Res.* **10**, 453–467 (2022).
11. D. Rifkin *et al.*, The role of LTBPs in TGFβ signaling. *Dev. Dyn.* **251**, 95–104 (2022).
12. R. O. Hynes, E. Ruoslahti, T. A. Springer, Reflections on integrins–Past, present, and future: The albert lasker basic medical research award. *JAMA* **328**, 1291–1292 (2022).
13. R. Wang *et al.*, GARP regulates the bioavailability and activation of TGF-β. *Mol. Biol. Cell* **23**, 1129–1139 (2012).
14. T. Oida, H. L. Weiner, Overexpression of TGF-ss 1 gene induces cell surface localized glucose-regulated protein 78-associated latency-associated peptide/TGF-ss. *J. Immunol.* **185**, 3529–3535 (2011).
15. P. H. Weinreb *et al.*, Function-blocking integrin αVβ6 monoclonal antibodies: Distinct ligand-mimetic and nonligand-mimetic classes. *J. Biol. Chem.* **279**, 17875–17887 (2004).
16. Z. Yang *et al.*, Absence of integrin-mediated TGFβ1 activation in vivo recapitulates the phenotype of TGFβ1-null mice. *J. Cell Biol.* **176**, 787–793 (2007).
17. X. Dong, N. E. Hudson, C. Lu, T. A. Springer, Structural determinants of integrin β-subunit specificity for latent TGF-β. *Nat. Struct. Mol. Biol.* **21**, 1091–1096 (2014).
18. X. Dong *et al.*, Force interacts with macromolecular structure in activation of TGF-β. *Nature* **542**, 55–59 (2017).
19. V. Q. Le *et al.*, Protection of the prodomain α1-helix correlates with latency in the transforming growth factor-β family. *J. Mol. Biol.* **434**, 167439 (2022).
20. J. P. Annes, Y. Chen, J. S. Munger, D. B. Rifkin, Integrin aVb6-mediated activation of latent TGF-β requires the latent TGF-β binding protein-1. *J. Cell Biol.* **165**, 723–734 (2004).
21. D. A. Calderwood *et al.*, The phosphotyrosine binding (PTB)-like domain of talin activates integrins. *J. Biol. Chem.* **277**, 21749–21758 (2002).
22. D. S. Harburger, M. Bouaouina, D. A. Calderwood, Kindlin-1 and -2 directly bind the C-terminal region of β integrin cytoplasmic tails and exert integrin-specific activation effects. *J. Biol. Chem.* **284**, 11485–11497 (2009).
23. P. Nordenfelt, H. L. Elliott, T. A. Springer, Coordinated integrin activation by actin-dependent force during T-cell migration. *Nat. Commun.* **7**, 13119 (2016).
24. C. McMahon *et al.*, Yeast surface display platform for rapid discovery of conformationally selective nanobodies. *Nat. Struct. Mol. Biol.* **25**, 289–296 (2018).
25. M. Shi *et al.*, Latent TGF-β structure and activation. *Nature* **474**, 343–349 (2011).
26. B. Zhao, S. Xu, X. Dong, C. Lu, T. A. Springer, Prodomain-growth factor swapping in the structure of pro-TGF-β1. *J. Biol. Chem.* **293**, 1579–1589 (2018).
27. S. Lienart *et al.*, Structural basis of latent TGF-β1 presentation and activation by GARP on human regulatory T cells. *Science* **362**, 952–956 (2018).
28. S. L. Nishimura, Integrin-mediated transforming growth factor-β activation, a potential therapeutic target in fibrogenic disorders. *Am. J. Pathol.* **175**, 1362–1370 (2009).
29. M. A. Travis, D. Sheppard, TGF-β activation and function in immunity. *Annu. Rev. Immunol.* **32**, 51–82 (2014).
30. I. B. Robertson, D. B. Rifkin, Regulation of the bioavailability of TGF-β and TGF-β-related proteins. *Cold Spring Harb. Perspect. Biol.* **8**, a021907 (2016).
31. Y. Qin *et al.*, A milieu molecule for TGF-β required for microglia function in the nervous system. *Cell* **174**, 156–171.e116 (2018).
32. K. Miyazono, A. Olofsson, P. Colosetti, C. H. Heldin, A role of the latent TGF-β1-binding protein in the assembly and secretion of TGF-β1. *Embo J.* **10**, 1091–1101 (1991).
33. B. X. Wu *et al.*, Glycoprotein A repetitions predominant (GARP) positively regulates transforming growth factor (TGF) β3 and is essential for mouse palatogenesis. *J. Biol. Chem.* **292**, 18091–18097 (2017).
34. S. Schumacher *et al.*, Structural insights into integrin α5β1 opening by fibronectin ligand. *Sci. Adv.* **7**, eabe9716 (2021).
35. J. Wang, Y. Su, R. E. Iacob, J. R. Engen, T. A. Springer, General structural features that regulate integrin affinity revealed by atypical αVβ8. *Nat. Commun.* **10**, 5481 (2019).
36. M. G. Campbell *et al.*, Cryo-EM reveals integrin-mediated TGF-β activation without release from latent TGF-β. *Cell* **180**, 490–501.e416 (2020).
37. O. Gotoh, Significant improvement in accuracy of multiple protein sequence alignments by iterative refinement as assessed by reference to structural alignments. *J. Mol. Biol.* **264**, 823–838 (1996).
38. X. Z. Huang *et al.*, Inactivation of the integrin β6 subunit gene reveals a role of epithelial integrins in regulating inflammation in the lung and skin. *J. Cell Biol.* **133**, 921–928 (1996).
39. S. L. Dallas *et al.*, Preferential production of latent transforming growth factor β-2 by primary prostatic epithelial cells and its activation by prostate-specific antigen. *J. Cell Physiol.* **202**, 361–370 (2005).
40. G. Jenkins, The role of proteases in transforming growth factor-β activation. *Int. J. Biochem. Cell Biol.* **40**, 1068–1078 (2008).
41. K. P. Conroy, L. J. Kitto, N. C. Henderson, αv integrins: Key regulators of tissue fibrosis. *Cell Tissue Res.* **365**, 511–519 (2016).
42. K. A. Riemondy *et al.*, Single cell RNA sequencing identifies TGFβ as a key regenerative cue following LPS-induced lung injury. *JCI Insight* **5**, e123637 (2019).
43. Y. Hao, D. Baker, P. Ten Dijke, TGF-β-mediated epithelial-mesenchymal transition and cancer metastasis. *Int. J. Mol. Sci.* **20**, 2767 (2019).
44. A. Ludlow *et al.*, Characterization of integrin β6 and thrombospondin-1 double-null mice. *J. Cell Mol. Med.* **9**, 421–437 (2005).
45. M. Guffroy *et al.*, Selective inhibition of integrin αvβ6 leads to rapid induction of urinary bladder tumors in cynomolgus macaques. *Toxicol Sci.* **192**, 130 (2023).
46. G. Raghu *et al.*, A Phase IIb randomized study of an Anti-αvβ6 monoclonal antibody in idiopathic pulmonary fibrosis. *Am. J. Respir. Crit. Care Med.* **206**, 1128–1139 (2022), 10.1164/rccm.202112-2824OC.
47. A. R. Aricescu, W. Lu, E. Y. Jones, A time- and cost-efficient system for high-level protein production in mammalian cells. *Acta Crystallogr. D. Biol. Crystallogr.* **62**, 1243–1250 (2006).
48. C. C. Liu, P. Leclair, S. Q. Yap, C. J. Lim, The membrane-proximal KXGFFKR motif of α-integrin mediates chemoresistance. *Mol. Cell Biol.* **33**, 4334–4345 (2013).
49. J. H. Kim *et al.*, High cleavage efficiency of a 2A peptide derived from porcine teschovirus-1 in human cell lines, zebrafish and mice. *PLoS One* **6**, e18556 (2011).
50. F. Mitjans *et al.*, An anti-α v-integrin antibody that blocks integrin function inhibits the development of a human melanoma in nude mice. *J. Cell Sci.* **108**, 2825–2838 (1995).
51. S. K. Akiyama, S. S. Yamada, W. T. Chen, K. M. Yamada, Analysis of fibronectin receptor function with monoclonal antibodies: Roles in cell adhesion, migration, matrix assembly, and cytoskeletal organization. *J. Cell Biol.* **109**, 863–875 (1989).
52. A. Artoni *et al.*, Integrin β3 regions controlling binding of murine mAb 7E3: Implications for the mechanism of integrin αIIbβ3 activation. *Proc. Natl. Acad. Sci. U.S.A.* **101**, 13114–13120 (2004).
53. O. J. Leger *et al.*, Humanization of a mouse antibody against human α4 integrin: A potential therapeutic for the treatment of multiple sclerosis. *Hum Antibodies* **8**, 3–16 (1997).
54. I. Hotzel *et al.*, A strategy for risk mitigation of antibodies with fast clearance. *MAbs* **4**, 753–760 (2012).
55. J. Takagi, H. P. Erickson, T. A. Springer, C-terminal opening mimics "inside-out" activation of integrin α5β1. *Nat. Struct. Biol.* **8**, 412–416 (2001).
56. P. J. Reeves, N. Callewaert, R. Contreras, H. G. Khorana, Structure and function in rhodopsin: High-level expression of rhodopsin with restricted and homogeneous N-glycosylation by a tetracycline-inducible N-acetylglucosaminyltransferase I-negative HEK293S stable mammalian cell line. *Proc. Natl. Acad. Sci. U.S.A.* **99**, 13419–13424 (2002).
57. A. Morin *et al.*, Collaboration gets the most out of software. *Elife* **2**, e01456 (2013).
58. K. Diederichs, XDSGUI (XDS WIki) (2022). https://wiki.uni-konstanz.de/xds/index.php/XDSGUI.
59. P. R. Evans, G. N. Murshudov, How good are my data and what is the resolution? *Acta Crystallogr. D. Biol. Crystallogr.* **69**, 1204–1214 (2013).
60. M. D. Winn *et al.*, Overview of the CCP4 suite and current developments. *Acta Crystallogr. D. Biol. Crystallogr.* **67**, 235–242 (2011).
61. S. Daopin, K. A. Piez, Y. Ogawa, D. R. Davies, Crystal structure of transforming growth factor-β2: An unusual fold for the superfamily. *Science* **257**, 369–373 (1992).
62. A. J. McCoy *et al.*, Phaser crystallographic software. *J. Appl. Crystallogr.* **40**, 658–674 (2007).
63. T. C. Terwilliger *et al.*, Iterative model building, structure refinement and density modification with the PHENIX AutoBuild wizard. *Acta Crystallogr. D Biol. Crystallogr.* **64**, 61–69 (2008).
64. P. Emsley, B. Lohkamp, W. G. Scott, K. Cowtan, Features and development of Coot. *Acta Crystallogr D. Biol. Crystallogr.* **66**, 486–501 (2010).
65. P. V. Afonine *et al.*, Towards automated crystallographic structure refinement with phenix.refine. *Acta Crystallogr. D Biol. Crystallogr.* **68**, 352–367 (2012).
66. I. W. Davis *et al.*, MolProbity: All-atom contacts and structure validation for proteins and nucleic acids. *Nucleic Acids Res.* **35**, W375–W383 (2007).
67. J. Li *et al.*, Conformational equilibria and intrinsic affinities define integrin activation. *EMBO J.* **36**, 629–645 (2017).
68. V.Q. Le, T.A. Springer, Crystal structure of human *pro*-TGF-beta2 in complex with Nb9, PDB. https://doi.org/10.2210/pdb8FXS/pdb. Deposited 25 January 2023.
69. V.Q. Le, T.A. Springer, Crystal structure of human *pro*-TGF-beta2 in complex with Nb18, PDB. https://doi.org/10.2210/pdb8FXV/pdb. Deposited 25 January 2023.

PNAS

Supporting Information for

A specialized integrin-binding motif enables proTGF-β2 activation by integrin αVβ6 but not αVβ8

Viet Q. Le[1,2,5], Bo Zhao[1,2,4,5], Siddanth Ramesh[1], Cameron Toohey[1], Adam DeCosta[1], Julian Mintseris[3], Xinyue Liu[3], Steven Gygi[3], Timothy A. Springer[1,2*]

Timothy A. Springer
Email: springer@crystal.harvard.edu

This PDF file includes:

Figures S1 to S5
Tables S1

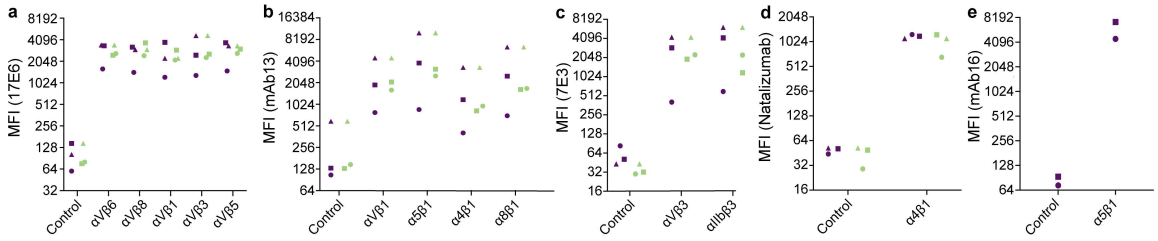

Fig. S1. Integrin cell surface expression. a–e, Median fluorescence intensities (MFIs) for integrin subunits on Expi293 cell transfectants used in co-culture assays with milieu anchor + TGF-β2 co-transfectants in Fig. 1a, b and Fig. S2a, b. MFIs are reported for staining with the αV-specific antibody 17E6 (**a**), β1-specific antibody mAb13 (**b**), β3-specfic antibody 7E3 (**c**), α4-specific antibody Natalizumab (**d**), and α5-specific antibody mAb16 (**e**). Each color and shape of symbol corresponds to an independent experiment with a matched control. Controls were transfected with an unrelated, non-crossreactive integrin.

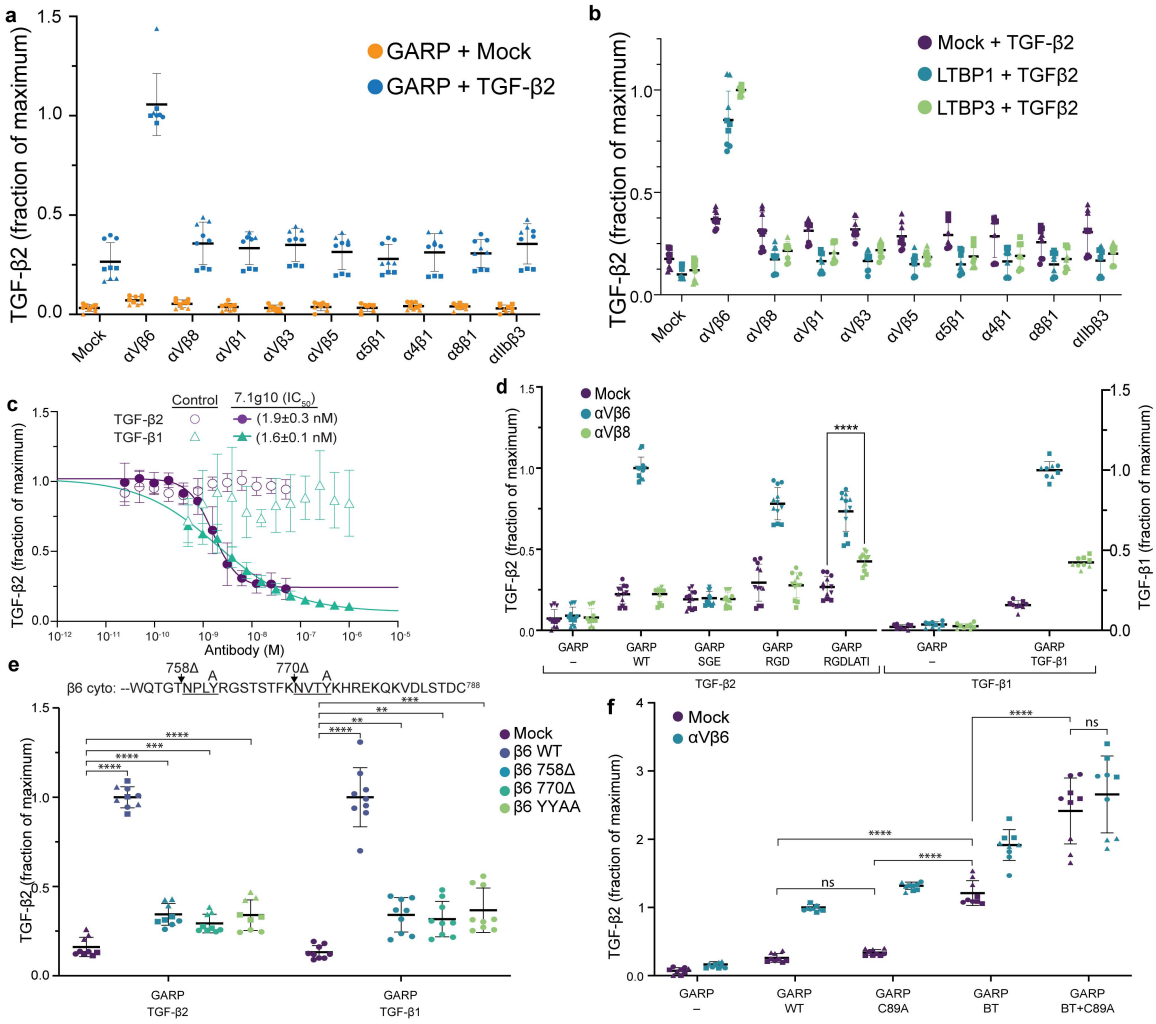

Fig. S2. Average results of TGF-β activation over multiple independent experiments. a–f, TGF-β activation over three independent experiments is shown as the fraction of activation in the presence of αVβ6 transfectants with GARP/TGF-β2 transfectants (a, c–f) or with LTBP3/TGF-β2 transfectants (b). TGF-β activation in each experiment was standardized using recombinant TGF-β2 growth factor except in panel (d), which used recombinant TGF-β2 or TGF-β1 growth factor. Triplicates in each experiment are shown as different points, with points in the same experiment shown as identical symbols (circles, squares or triangles) along with the mean (a–b,d–f) or mean±standard deviation from three independent experiments are shown (c). p-values were determined using the Tukey multiple comparisons test following a two-way ANOVA (ns: $p > 0.05$, *: $p < 0.05$, **: $p < 0.01$, ***: $p < 0.001$, ****: $p<0.0001$). **a, b**, All experiments on integrin-dependence of activation related to Fig. 1a, b. **c**, Inhibition of αVβ6-mediated activation of TGF-β2 and TGF-β1 by the αVβ6 function-blocking antibody 7.1g10 related to Fig. 1d. **d**, Effect of mutations to the SGDQKTI motif in TGF-β2 on αVβ6-mediated activation. Related to Fig. 1e. **e**, Effect of truncations and mutations that eliminate talin or kindlin binding sites in the integrin β6 cytoplasmic domain on TGF-β2 activation. Related to Fig. 1f. **f**, Effect of Cys-to-Ala mutations that disrupt TGF-β2 inter-prodomain disulfides on αVβ6-mediated activation. BT, all three bowtie cysteines. Related to Fig. 1g.

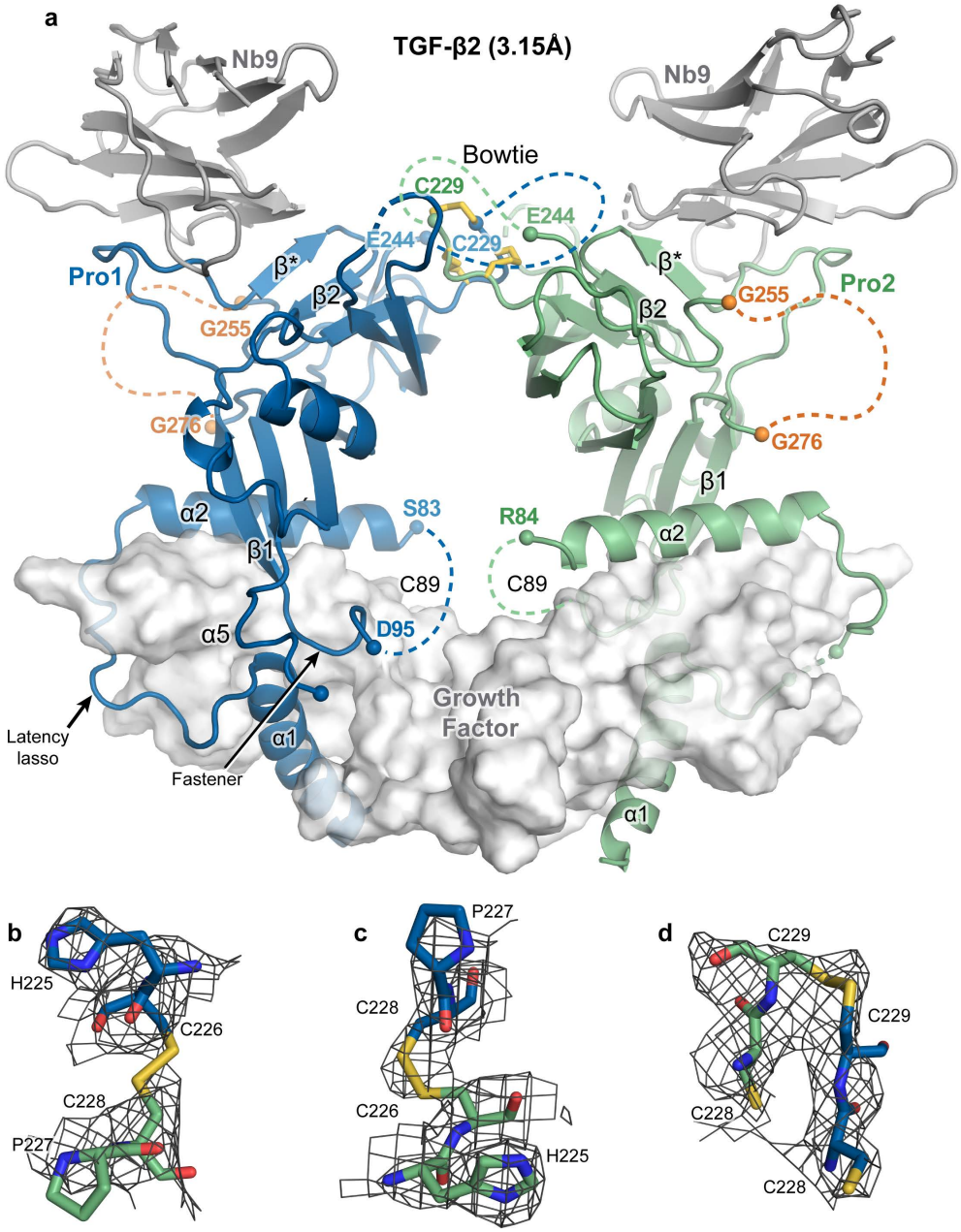

Fig. S3. Crystal structure of the proTGF-β2/Nb9 complex at 3.15 Å. a, Nanobodies and prodomains are shown in ribbon cartoon, whereas the growth factor dimer is shown as a transparent solvent-accessible surface. Disulfides are shown in yellow stick. The termini that flank disordered regions are indicated by spheres. The disordered SGD-containing loops of TGF-β2 are depicted as orange dashes. **b–d**, The three bowtie disulfides (yellow) and flanking residues of TGF-β2 are shown in stick with black mesh showing the 2Fo–Fc map contoured at 1σ.

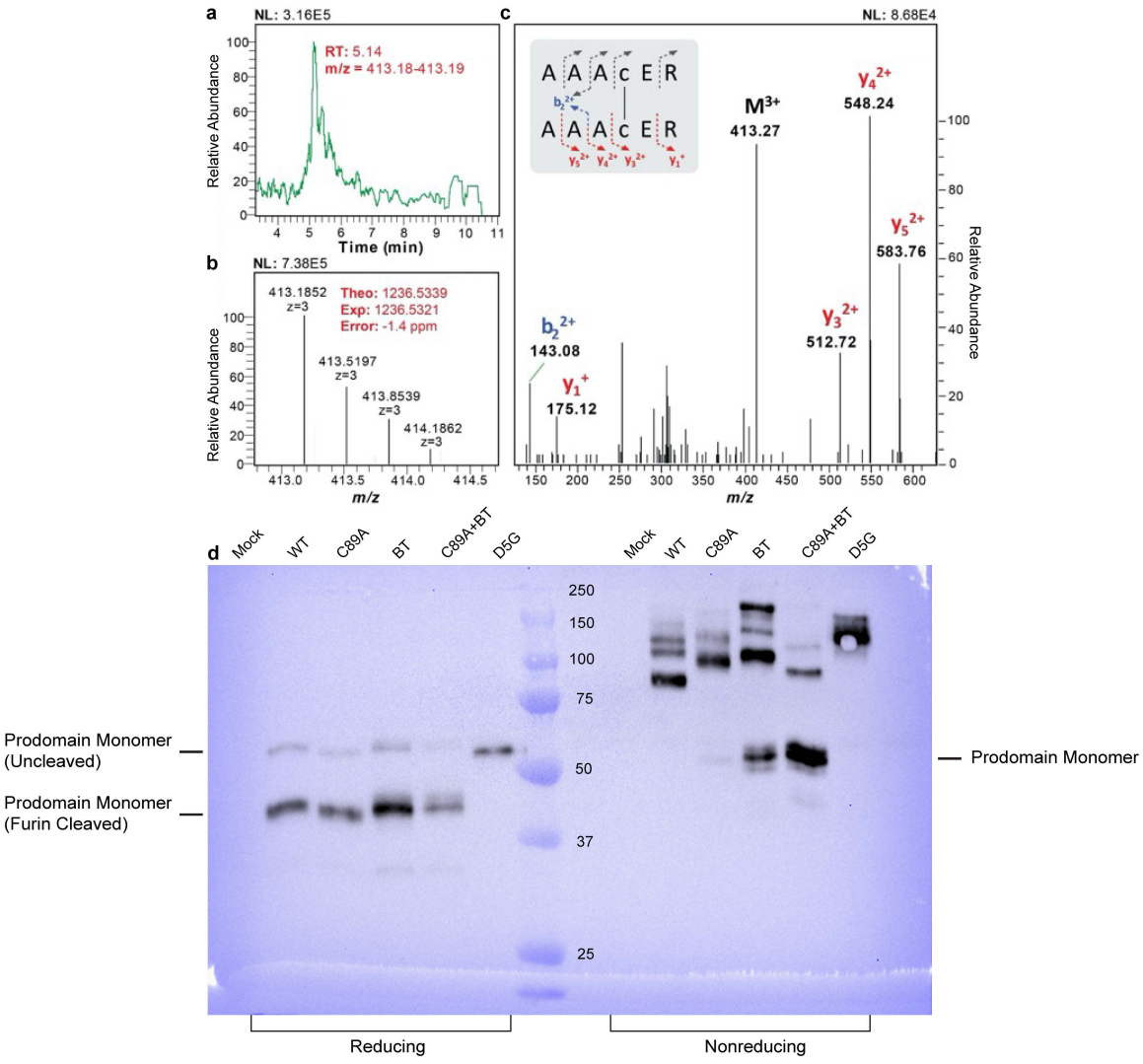

Fig. S4. Mass spectrometry and mutational evidence for the Cys-89 inter-prodomain disulfide. a–c, Mass spectrometry data on the disulfide-linked tryptic peptide bearing Cys-89. **a**, Extracted ion chromatogram (EIC) of the peptide. The $(M + 3H)^{3+}$ ion was extracted with a mass/charge ratio (m/z) range of 413.18-416.19. **b**, MS1 spectrum of the triply charged peptide with the first four isotopic peaks shown. Exact mass calculated based on the monoisotopic peak (m/z = 413.1852, z = 3) was 1236.5321, with the observed mass shift of 1.4 parts per million (ppm). **c**, Tandem mass (MS/MS) spectrum of the precursor peptide (MH33+, m/z = 413.1852) was acquired with higher-energy C-trap dissociation on an Orbitrap Exploris mass spectrometer. Dissociation of the two identical disulfide-linked peptides results in the same fragment ions. Identified ions are annotated in the spectrum as N-terminal (b-type ions) and C-terminal (y-type ions). **d**, Anti-His western blot of conditioned supernatant from mock, WT, and mutant TGF-β2 transfectants under reducing (left) and non-reducing (right) conditions. BT, bowtie mutant (C226A, C228A, C229A). A mutant with abolished PC/furin cleavage (D5G) was used as a control for uncleaved monomers and dimers. The higher molecular weight bands (>75 kDa) still present in non-reducing SDS-PAGE for the C89A+BT mutant are likely to be furin-unprocessed proTGF-β2 dimers that are disulfide linked via their growth factor domains; a faint uncleaved C89A+BT prodomain-GF monomer band is also seen in reducing SDS-PAGE.

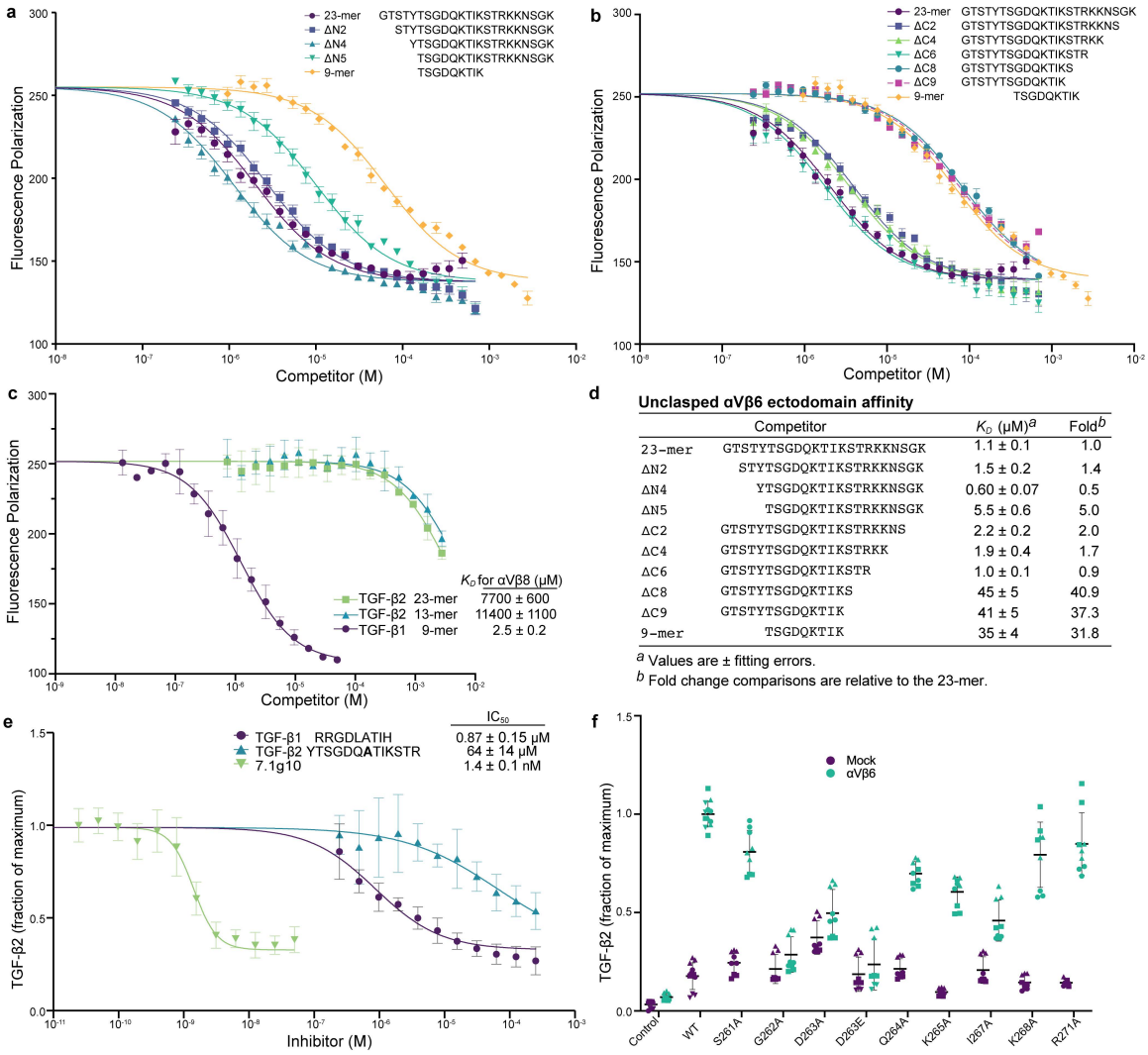

Fig. S5. The binding site within TGF-β2 for integrin αVβ6. a–c, Fluorescence polarization assays showing the effect of competitors on binding of 10 nM FITC-TGF-β3 GRGDLGRLK peptide to 20 nM αVβ6 ectodomain (a, b) or to 200 nM αVβ8 ectodomain (c). Data points show mean±standard error of three independent experiments (five for the 23-mer and 9-mer in panels A and B) each performed in duplicate and were fitted to a variable slope (four parameter) dose response curve. Panels (a) and (b) display the same data for the 23-mer and the 9-mer. **d**, Summary of K_Ds determined in (a) and (b). **e, f**, TGF-β activation over three independent experiments is shown as the fraction of TGF-β released in the presence of αVβ6 transfectants from GARP/TGF-β2 transfectants. Data are mean±standard deviation from three independent experiments (e) or each triplicate result in each experiment as a different point, with points in the same experiment shown as identical symbols along with the mean±standard deviation (f). **e**, Inhibition of αVβ6-mediated activation of TGF-β2 by the K265A 13-mer TGF-β2 peptide compared to the 9-mer TGF-β1 peptide. The αVβ6 function-blocking antibody 7.1g10 was used as a positive control. Data were fit to a variable slope (four parameter) dose response curve to calculate IC_{50} values. Related to Fig. 3e. **f**, Effect of Ala mutations in the integrin αVβ6-binding motif on TGF-β2 activation in CAGA luciferase reporter co-culture assays. Related to Fig. 3f.

	TGF-β2/Nb18	TGF-β2/Nb9
Data Collection		
Space group	P 2_1 2 2_1	P 1 2_1 1
Cell dimensions		
a, b, c (Å)	70.75, 78.16, 88.89	69.683, 89.554, 89.74
α, β, γ (°)	90.0, 90.0, 90.0	90.0, 95.0, 90.0
Resolution (Å)	44.44–2.2 (2.279–2.2)	48.27–3.15 (3.263–3.15)
R-merge	0.1466 (2.61)	0.2415 (1.482)
I/σ (I)	10.11 (0.76)	8.48 (1.45)
$CC_{1/2}$	0.998 (0.212)	0.967 (0.423)
Unique reflections	25659 (2538)	18955 (1881)
Completeness (%)	99.79 (99.84)	98.27 (99.37)
Multiplicity	6.5 (6.5)	3.4 (3.6)
Refinement		
Monomers/ASU	2 (1 TGF-β2 and 1 Nb)	4 (2 TGF-β2 and 2 Nb)
Resolution (Å)	44.44–2.2	48.27–3.15
No. reflections for R-free	1255 (124)	1908 (183)
R_{work} (%)	0.2266 (0.349)	0.2495 (0.3619)
R_{free} (%)	0.2491 (0.3698)	0.3010 (0.3968)
No. atoms		
Protein	3469	6678
Ligand/ion	27	54
Water	63	4
Average overall *B*-factor	60.32	89.76
Protein	60.40	89.73
Ligand/ion	64.6	100.02
Water	54.60	63.01
RMSD		
Bond lengths (Å)	0.005	0.002
Bond angles (°)	0.75	0.54
Ramachandran analysis[a]		
Favored (%)	96.12	93.43
Allowed (%)	3.88	6.31
Outliers (%)	0	0.26
MolProbity percentile[a] Clash/Geometry	100^{th}/99^{th}	100^{th}/100^{th}
PDB	8FXV	8FXS

Table S1. Data collection and refinement statistics.
Values in parentheses correspond to the statistics in the highest resolution bin.
RMSD, root-mean-square deviation. [a]Calculated with MolProbity.